Journal of Hydroscience and Hydraulic Engineering
Vol. 26, No.1 May, 2008, 73-89

Numerical simulation on local scouring around a spur dike using various turbulence and sediment transport models

By

Shinichiro Onda

Department of Urban Management, Kyoto University, Nishikyo, Kyoto, Japan

Takashi Hosoda

Department of Urban Management, Kyoto University, Nishikyo, Kyoto, Japan

Ichiro Kimura

Department of Civil and Environmental Engineering,
Matsue National College of Technology, Matsue, Japan

and

Michiaki Iwata

CTI Engineering Co., Ltd., Osaka, Japan

SYNOPSIS

Local scouring tends to occur around spur dikes. Therefore, it is important to estimate not only the maximum scour depth, but also the bed geometry around them. In this study, local scouring around a dike was simulated by means of various turbulence and sediment transport models. The standard and non-linear k-ε models were adopted as the turbulence model, with equilibrium and non-equilibrium sediment transport models. To evaluate the performance of the model, calculated results were compared with the results of experiments conducted by Michiue and Hinokidani (18); and the applicability of all these models was assessed by examining the temporal variation of the flow near the bed and the variation of the bed level. A comparison was made between the equilibrium and non-equilibrium sediment transport models. It revealed that the temporal variation of the bed elevation in the initial scouring process and the bed geometry in the equilibrium stage were different.

INTRODUCTION

Local scouring occurs around spur dikes, and the estimation of maximum scour depth is important in terms of mitigating the destruction of structures. On the other hand, certain characteristics of dikes have been found to produce aquatic habitats. Therefore, from the viewpoint of ecological problems as well as mitigating disasters, it is

of paramount importance to predict accurately not only the maximum scour depth, but also the bed geometry around dikes.

Numerous experimental studies concerning flows and bed deformation around dikes have been conducted. Ikeda et al. (11) examined the momentum exchange rate between the main flow and the spur dike regions around the impermeable spur dikes. Ishigaki et al. (12) and Tominaga and Matsumoto (26) pointed out that the angle of dike affects the position of scouring and deposition.

A number of computations have been performed considering only the flow around the spur dikes (Ikeda et al. (11), Muneta and Shimizu (19), Kimura et al. (15), (17)); on the other hand, some computations considered bed deformation with the flow simulation around spur dikes (Fukuoka et al. (3), (4), (5), Michiue and Hinokidani (18), Yossef and Rupprecht (29), Zhang et al. (30)). Flow models used in previous studies are classified as follows: (a) a plane 2D model (Ikeda et al. (11), Yossef and Rupprecht (29)); (b) a refined 2D model, including the local transformation of velocity distribution or the force due to dikes (Muneta and Shimizu (19), Fukuoka et al. (3), (4)) and (c) a fully 3D model (Michiue and Hinokidani (18), Fukuoka et al. (5), Kimura et al. (15), (17), Zhang et al. (30)). For the bed deformation, equilibrium sediment transport models are generally applied; for example, Meyer-Peter-Muller and Hasegawa (8) formulas are used to calculate bed-load flux in the streamwise and the transversal directions, respectively. In their studies, the applicability of numerical models is examined through the comparison with experimental results. Kimura et al. (17) simulated the flow around the dikes under various hydraulic conditions, and investigated the effects of the inclination angle and the ratio of the spacing between two dikes to the length. They reported that the flow patterns were in close agreement with observations for the case of fully 3D models. However, in many studies concerning bed deformation, the maximum scour depth is underestimated, and the position of scouring and deposition could not be reproduced well. The reason for this is that the turbulence, sediment transport models, and the calculations of sediment sliding are not employed correctly. Moreover, in some models, the assumption of hydrostatic pressure distribution is used, but it is not applicable in such cases.

Nagata et al. (20) have applied a fully 3D computational model, with the nonlinear k-ε turbulence model and the equation of motion of sediment particles in the non-equilibrium sediment transport model to simulate flow and bed deformation around a spur dike and bridge pier. They showed that the model could predict the bed topography better than the previous models; however, since they focused on the bed geometry in the equilibrium stage, the temporal variation of scouring processes under the various turbulence and bed deformation models was not examined in detail.

In this study, local scouring around a dike is simulated by using various turbulence and sediment transport models to gain a better understanding of their applicability. The numerical results are compared with the experiments conducted by Michiue and Hinokidani (18); and the applicability of these models is verified by examining the temporal variation of flow near the bed and the bed variations.

NUMERICAL MODEL

Basic equations of flow model

The Reynolds averaged 3D flow model in a generalized curvilinear moving coordinate system is applied to simulate the flow fields. The basic equations are expressed as follows:

[Continuity equation]

$$\frac{\partial}{\partial \xi^i}\left(\frac{U^i}{J}\right)=0 \tag{1}$$

[Momentum equation]

$$\frac{\partial}{\partial t}\left(\frac{U^i}{J}\right)+\frac{\partial}{\partial \xi^j}\left(\frac{\left(U^j-U_G^j\right)U^i}{J}\right)-\frac{\left(U^j-U_G^j\right)\mathbf{u}}{J}\cdot\frac{\partial}{\partial \xi^j}\left(\nabla\xi^i\right)-\frac{\mathbf{u}}{J}\cdot\frac{\partial}{\partial t}\left(\nabla\xi^i\right)$$
$$=-\frac{g^{ij}}{\rho J}\frac{\partial p}{\partial \xi^j}+\frac{\mathbf{f}}{J}\cdot\nabla\xi^i+\frac{1}{J}\frac{\partial \xi^j}{\partial x_m}\frac{\partial \xi^i}{\partial x_l}\frac{\partial}{\partial \xi^j}\left(\tau_{lm}-\overline{u_l'u_m'}\right) \tag{2}$$

[k-equation]

$$\frac{\partial}{\partial t}\left(\frac{k}{J}\right)+\frac{\partial}{\partial \xi^j}\left(\frac{\left(U^j-U_G^j\right)k}{J}\right)=\frac{-\overline{u_i'u_j'}}{J}\frac{\partial \xi^l}{\partial x_j}\frac{\partial u_i}{\partial \xi^l}-\frac{\varepsilon}{J}+\frac{\partial}{\partial \xi^l}\left(\left(\nu+\frac{D_t}{\sigma_k}\right)\frac{g^{lm}}{J}\frac{\partial k}{\partial \xi^m}\right) \tag{3}$$

[ε-equation]

$$\frac{\partial}{\partial t}\left(\frac{\varepsilon}{J}\right)+\frac{\partial}{\partial \xi^j}\left(\frac{\left(U^j-U_G^j\right)\varepsilon}{J}\right)$$
$$=C_{\varepsilon 1}\frac{\varepsilon}{k}\frac{\left(-\overline{u_i'u_j'}\right)}{J}\frac{\partial \xi^l}{\partial x_j}\frac{\partial u_i}{\partial \xi^l}-\frac{C_{\varepsilon 2}}{J}\frac{\varepsilon^2}{k}+\frac{\partial}{\partial \xi^l}\left(\left(\nu+\frac{D_t}{\sigma_\varepsilon}\right)\frac{g^{lm}}{J}\frac{\partial \varepsilon}{\partial \xi^m}\right) \tag{4}$$

in which

$$U^i\equiv\left(\partial\xi^i/\partial x_j\right)u_j \tag{5a}$$

$$U_G^i\equiv\left(\partial\xi^i/\partial x_j\right)u_{jG} \tag{5b}$$

$$\nabla\equiv\left(\partial/\partial x_1,\partial/\partial x_2,\partial/\partial x_3\right) \tag{5c}$$

$$g^{ij}\equiv\nabla\xi^i\cdot\nabla\xi^j \tag{5d}$$

$$\tau_{ij}\equiv\nu\left(\frac{\partial \xi^m}{\partial x_j}\frac{\partial u_i}{\partial \xi^m}+\frac{\partial \xi^m}{\partial x_i}\frac{\partial u_j}{\partial \xi^m}\right) \tag{5e}$$

where t = time; (x_1, x_2, x_3) = Cartesian coordinates (x_3 indicates the vertical coordinate); (ξ_1, ξ_2, ξ_3)= generalized curvilinear coordinates; J = Jacobian of transformation; g^{ij} = contravariant metric tensors; U^i = contravariant components of flow velocity vector; $U^i{}_G$ = contravariant components of grid velocity vector; $\mathbf{u}$ = velocity vector [= (u_1, u_2, u_3)]; u_i = velocity components in Cartesian coordinates; u_{iG} = grid velocity components in Cartesian coordinate; p = pressure; $\mathbf{f}$ = gravitational vector [= (0, 0, -g)]; g = gravitational acceleration; τ_{ij} = viscous stress tensors; $-\overline{u_i'u_j'}$ = Reynolds stress tensors; k = turbulent kinetic energy; ε = dissipation rate; ρ = fluid density; ν = kinematic viscosity of fluid; and i, j, k, l each denotes the value of 1, 2 and 3.

A second order nonlinear k-ε model is applied as the turbulence model to simulate complex turbulent flows with separation. The applicability of this model is examined by simulating the flow around a square cylinder (Kimura and Hosoda (16)) and a spur dike (Kimura et al. (15), (17), Nagata et al. (20)).

$$-\overline{u_i'u_j'} = D_t\left(\frac{\partial \xi^m}{\partial x_j}\frac{\partial u_i}{\partial \xi^m}+\frac{\partial \xi^m}{\partial x_i}\frac{\partial u_j}{\partial \xi^m}\right)-\frac{2}{3}k\delta_{ij}-\frac{k}{\varepsilon}D_t\sum_{\beta=1}^{3}C_\beta\left(S_{\beta ij}-\frac{1}{3}S_{\beta\alpha\alpha}\delta_{ij}\right) \quad (6)$$

$$D_t = C_\mu\frac{k^2}{\varepsilon} \quad (7a)$$

$$S_{1ij}=\frac{\partial u_i}{\partial x_r}\frac{\partial u_j}{\partial x_r},\quad S_{2ij}=\frac{1}{2}\left(\frac{\partial u_r}{\partial x_i}\frac{\partial u_j}{\partial x_r}+\frac{\partial u_r}{\partial x_j}\frac{\partial u_i}{\partial x_r}\right),\quad S_{3ij}=\frac{\partial u_r}{\partial x_i}\frac{\partial u_r}{\partial x_j} \quad (7b)$$

where D_t = eddy viscosity coefficient. Eqs. 6 and 7 are equivalent to the expressions reported by Gatski and Speziale (6). Other coefficients C_1, C_2, C_3 and C_μ are described as follows:

$$C_1=\frac{0.4}{1+0.01M^2}, C_2=0.0, C_3=\frac{-0.13}{1+0.01M^2} \quad (8a)$$

$$M=\max(S,\Omega) \quad (8b)$$

$$S=\frac{k}{\varepsilon}\sqrt{\frac{1}{2}\left(\frac{\partial u_i}{\partial x_j}+\frac{\partial u_j}{\partial x_i}\right)^2}, \Omega=\frac{k}{\varepsilon}\sqrt{\frac{1}{2}\left(\frac{\partial u_i}{\partial x_j}-\frac{\partial u_j}{\partial x_i}\right)^2} \quad (8c)$$

$$C_\mu=\min\left[0.09, 0.3/(1+0.09M^2)\right] \quad (9)$$

Eqs. 8 are adjusted by comparing the turbulent intensity distribution in a simple shear flow (Kimura and Hosoda (16)). Eq. 9 is determined in order to satisfy the realizability in a simple shear flow and the singular points in both 2D and 3D flow fields (Hosoda et al (10)).

In this study, a standard k-ε model is also applied in order to compare numerical results with nonlinear k-ε model.

Bed deformation model

Non-equilibrium sediment transport model

The equilibrium and non-equilibrium sediment transport models are applied to calculate the bed variation to examine their applicability. Firstly, the non-equilibrium sediment transport model (Nagata et al. (20)) is described. This model consists of four steps: (i) evaluation of pick-up rate and volume of pick-up sediment; (ii) calculation of the trajectory of sediment movements by solving an equation of motion of sand particles; (iii) calculation of sediment deposition volume; and (iv) the temporal variation of bed elevation.

The pick-up rate p_s is evaluated by the following equation proposed by Nakagawa et al. (21), where the effect of local bed slope on sediment motion is included. To obtain the dimensionless tractive stress, the bed shear velocities are determined from the logarithmic velocity profile.

$$p_s\sqrt{\frac{d}{(\sigma/\rho-1)g}}=F_0G_*\tau_*\left(1-\frac{k_p\Phi\tau_{*c}}{\tau_*}\right)^{m_p} \quad (10a)$$

$$G_* = \frac{\cos\Psi + k_L\mu_s}{1+k_L\mu_s} \tag{10b}$$

$$\Phi = \left(\frac{\mu_s\cos\theta_b - \sin\theta_b\cos\alpha}{\cos\Psi + k_L\mu_s}\right)\left(\frac{1+k_L\mu_s}{\mu_s}\right) \tag{10c}$$

where p_s = pick-up rate; d = diameter of sediment particle; τ_* = dimensionless tractive stress[= $u_*^2/(\sigma/\rho\text{-}1)gd$]; u_* = bed shear velocity; τ_{*c} = dimensionless critical tractive stress proposed by Iwagaki (13); G_* = the coefficient of directional deviation between velocity near bed and sediment movement vectors; Φ = the coefficient of side bank slope; μ_s = static friction factor (=0.7); k_L = ratio of lift force to drag force (=0.85); θ_b = the local bed slope angle; ψ = the angle between velocity vector near bed and sediment movement direction; α = the angle between direction of maximum local bed slope and sediment movement direction; and F_0, k_p, and m_p = constants (=0.03, 0.7, and 3, respectively).

By using the above pick-up rate, the volume of sediment pick-up per unit time V_p can be calculated as follows:

$$V_p = \frac{A_3 d}{A_2} p_s S_p, \quad S_p = \frac{\partial\xi^3/\partial x_3}{J} \tag{11}$$

where A_2, A_3 = the shape characteristics of sand grain for two- and three- dimensional geometrical properties (= $\pi/4$, $\pi/6$); S_p = area of bed surface mesh.

To calculate the sediment movement, the unit vectors $\mathbf{p}_{b1}$ and $\mathbf{p}_{b2}$ are defined, which are parallel to the local bed surface on (x_1-x_3) and (x_2-x_3) planes, respectively.

$$\mathbf{p}_{b1} = \begin{pmatrix}\cos\theta_{b1}\\ 0\\ \sin\theta_{b1}\end{pmatrix}, \quad \mathbf{p}_{b2} = \begin{pmatrix}0\\ \cos\theta_{b2}\\ \sin\theta_{b2}\end{pmatrix} \tag{12}$$

where θ_{b1}, θ_{b2} = angles of bed inclination in the x_1 and x_2 directions, respectively. To calculate the trajectory of sediment movements, the momentum equation of sand particles in the $\mathbf{p}_{bi}$ (i=1, 2) direction is solved.

$$\rho\left(\frac{\sigma}{\rho}+C_m\right)A_3 d^3\frac{du_{sedi}}{dt} = D_i + W_i - F_i \tag{13}$$

$$D = \frac{C_D\rho}{2}\left(u_{bi}-u_{sedi}\right)^2 c_e A_2 d^2 \tag{14a}$$

$$W = (\sigma-\rho)gA_3 d^3 \tag{14b}$$

$$F = \mu_k\left(W\frac{\cos\theta_{b1}\cos\theta_{b2}}{\sin\theta_p} - k_L D\right) \tag{14c}$$

where C_m = coefficients of added mass (=0.5); u_{sedi} = sediment particle velocity in the $\mathbf{p}_{bi}$ direction; D = fluid drag force on a sediment particle; W = submerged weight of a sediment particle; F = the friction force between sediment particle and bed; D_i, W_i, F_i = direction components of D, W and F; u_{bi} = fluid velocity near the bed at the distance of $k_d d$ from bed; k_d = constant (=0.8); C_D = drag coefficients =(0.4); μ_k = kinetic friction factor (=0.35); and θ_p = angle between $\mathbf{p}_{b2}$ and $\mathbf{p}_{b1}$.

The position vector of the sediment particles $\mathbf{p}_{sed(n)}$ at n-th step after sediments being picked up can be calculated using the vector of sediment particle velocity u_{sedi}. Thus, the distance of sediment movement $s_{(n)}$ can be calculated.

$$\mathbf{p}_{sed(n)} = \mathbf{p}_{sed(n-1)} + \Delta t \cdot \mathbf{u}_{sed} \tag{15}$$

$$s_{(n)} = \sum \Delta t \left| \mathbf{u}_{sed(n)} \right| \tag{16}$$

The deposition volume $V_{d(j,\,n)}$ of sediment moving from point j after n-th step can be obtained using the probability density function of step length.

$$V_{d(j,n)} = V_{p(j)} f_s\left(s_{(n)}\right) \left| \mathbf{u}_{sed} \right| \Delta t \tag{17a}$$

$$f_s\left(s_{(n)}\right) = \frac{1}{\lambda} \exp\left(-\frac{s_{(n)}}{\lambda} \right) \tag{17b}$$

where $V_{p(j)}$ = volume of pick-up sediment at point j; $f_s(s_{(n)})$ = the probability density function of step length; and λ = averaged step length. To estimate λ, the equation proposed by Einstein (2) is adopted. It should be noted that while the position of sediment pick-up is at the center of the mesh, the point of sediment deposition does not coincide with the pick-up position.

Thus, the position of deposition can be found by using the position vector (Eq. 15); and the total deposition volume is distributed to each grid point. Using the pick-up and deposition volumes calculated by Eqs. 11 and 17, the temporal variation in the bed elevation can be obtained.

$$\frac{\partial z_b}{\partial t} = \frac{A_1 A_2}{A_3} \frac{\left(V_d - V_p\right)}{S_d} \tag{18}$$

where z_b = bed elevation; A_1 = the shape coefficient of sand grain for one dimensional geometrical properties (=1.0); and S_d = area of bed surface mesh where sediment is deposited.

Equilibrium sediment transport model

In the equilibrium sediment transport model, the empirical bed-load transport formula, such as Meyer-Peter Muller or Ashida & Michiue formula, is usually used. However, in order to maintain the same critical value of sediment movement in the equilibrium and non-equilibrium sediment transport models, such kinds of empirical formula are not used in this study. Instead, the bed-load transport flux q_{Bs} is calculated by using the pick-up rate (Eqs.10). Thus, the bed-load flux q_{Bn} in the transversal direction (Hasegawa (8)) can be obtained from Eq. 19b. The temporal variation of the bed elevation is calculated by Eq. 19c, after the bed-load fluxes (Eqs. 19a and 19b) are transformed to the ones in the generalized curvilinear coordinates.

$$q_{Bs} = \frac{A_3}{A_2} p_s \Lambda d \tag{19a}$$

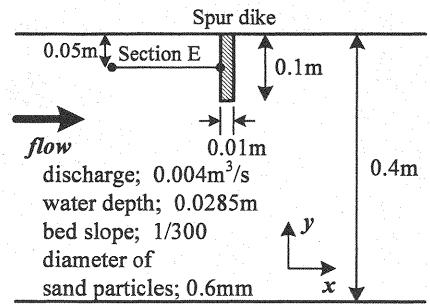

Fig. 1 Experimental condition by Michiue and Hinokidani (18)

Table 1 Computational conditions

	bed deformation model	turbulence model
Case1	non-equilibrium sediment transport model	nonlinear k-ε model
Case2	equilibrium sediment transport model	nonlinear k-ε model
Case3	non-equilibrium sediment transport model	standard k-ε model

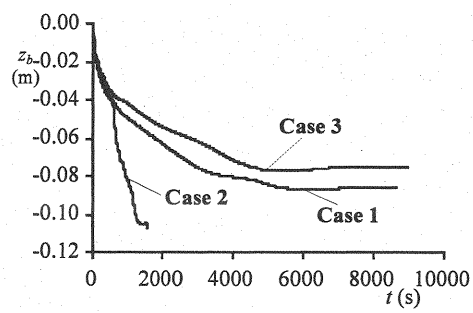

Fig. 2 Temporal variation of maximum scour depths

$$q_{Bn} = q_{Bs}\left(-\frac{\partial z_b}{\partial n}\sqrt{\frac{\tau_{*c}}{\mu_s \mu_k \tau_*}}\right) \tag{19b}$$

$$\frac{\partial}{\partial t}\left(\frac{z_b}{J}\right) + \frac{1}{1-\delta}\left\{\frac{\partial}{\partial \xi}\left(\frac{q_B^{\xi}}{J}\right) + \frac{\partial}{\partial \eta}\left(\frac{q_B^{\eta}}{J}\right)\right\} = 0 \tag{19c}$$

where Λ = averaged step length (=100d); and δ = porosity.

Sliding of bed materials

A scour hole is developed and the local bed slope in the scour hole becomes steep. In the previous study (18), it is reported that the sliding of bed materials occurs around the dike, when the local bed slope exceeds a critical value, $\theta_{b\max}$. In this study, the calculation of sliding is integrated. The critical slope angle is estimated to be the angle of repose of bed materials.

Details of the numerical method and procedures for calculating are described in the reference (Nagata et al. (20)) and are skipped in this paper.

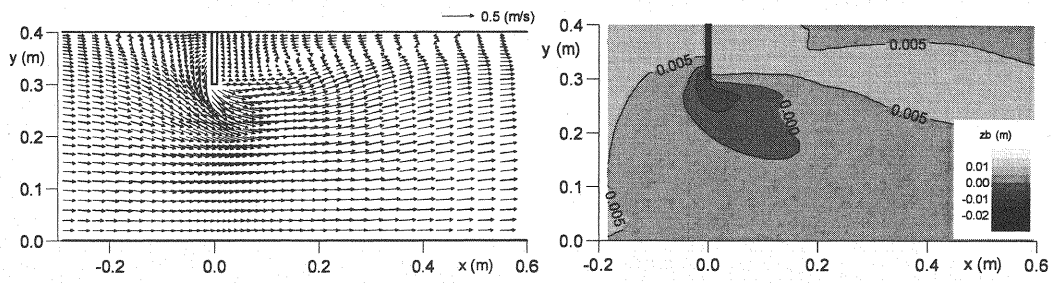

(a) t = 60 (s)

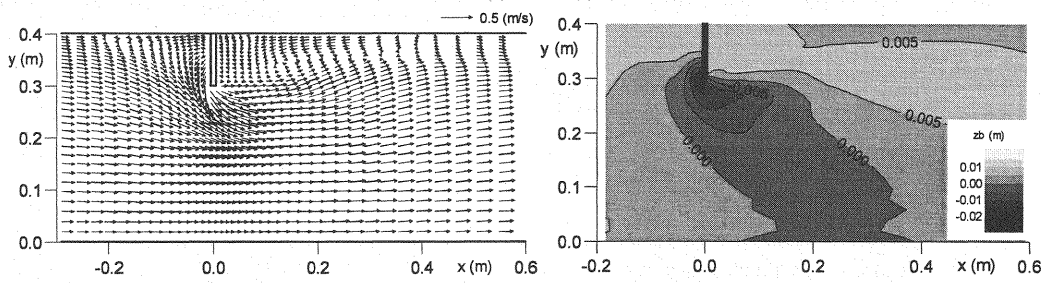

(b) t = 120 (s)

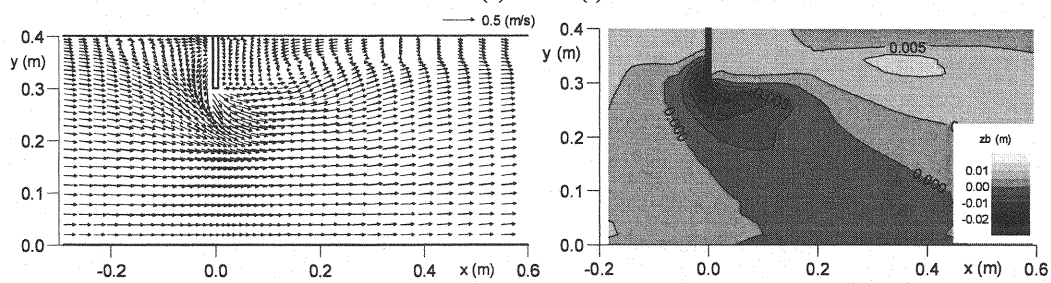

(c) t = 180 (s)

Fig. 3 Temporal variation of flows near bed and bed elevation contours (Case 1)

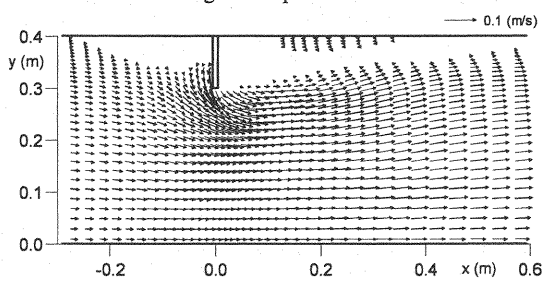

Fig. 4 Velocity vectors of sediment particles just after picked up at t = 60(s)

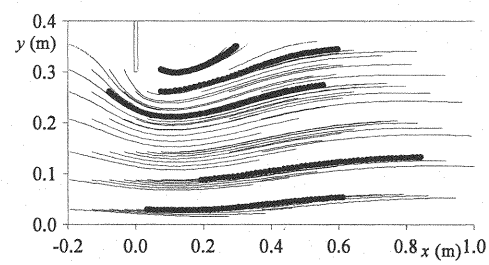

Fig. 5 Trajectories of sediment movements picked up at t = 60(s)

APPLICATION

The numerical model is applied to the experiments of flow and bed deformation around a spur dike conducted by Michiue and Hinokidani (18). The experimental setup and hydraulic conditions are illustrated in Figure 1. In this investigation, three cases are tested by incorporating different turbulence and sediment transport models, as shown in Table 1. Δt is equal to 0.005 (s) in Case 1 and 3; and 0.002 (s) in Case 2, and it took about 2 weeks to obtain the numerical results in each equilibrium stage. The purpose is to examine the appropriate combination of turbulence

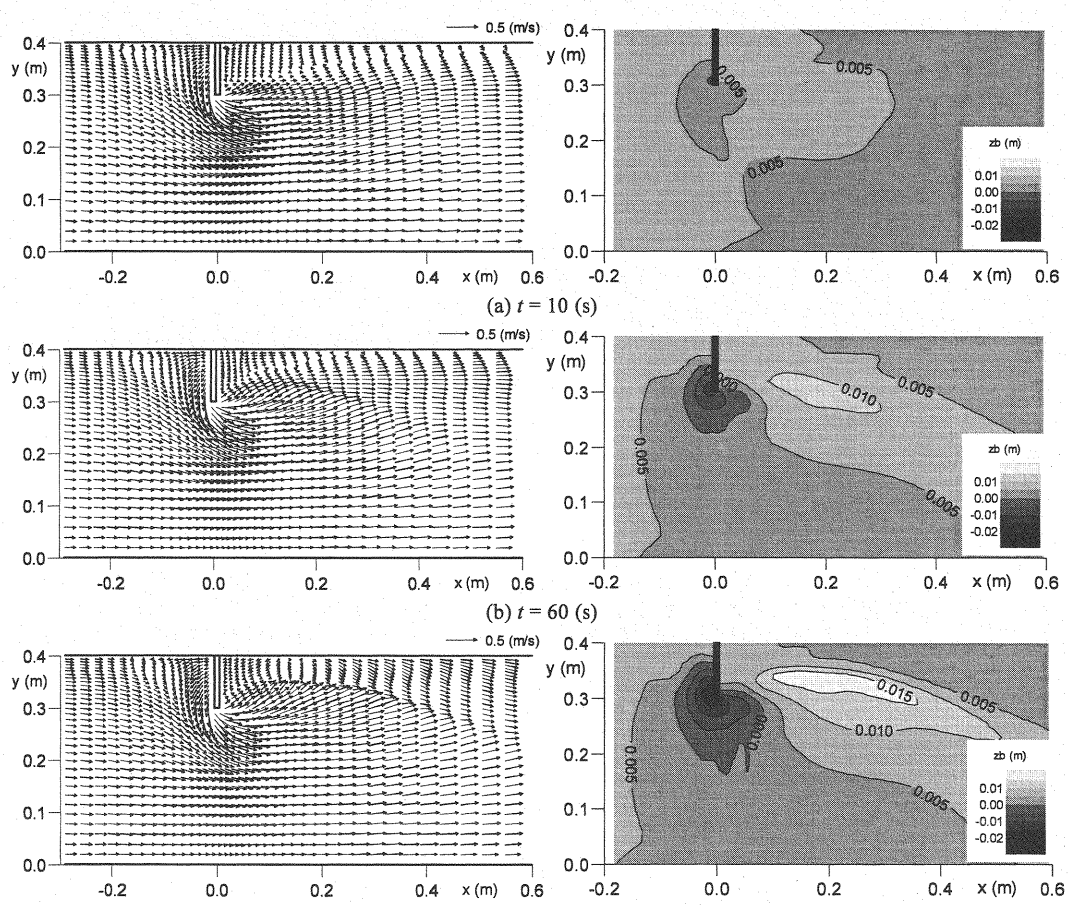

(a) t = 10 (s)

(b) t = 60 (s)

(c) t = 120 (s)

Fig. 6 Temporal variation of flows near bed and bed elevation contours (Case 2)

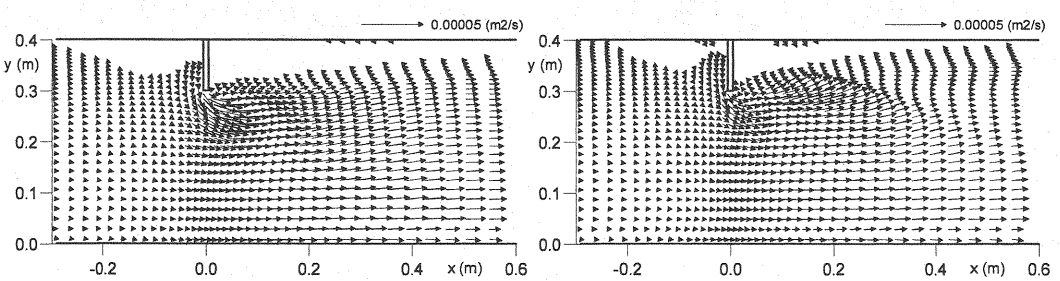

Fig. 7 Temporal variation of bed-load flux vectors (left: t = 10 (s), right: t = 60 (s))

and bed deformation models.

RESULTS AND DISCUSSIONS

Figure 2 shows the temporal variation of maximum scour depths for all the cases. It is clear that the equilibrium stages for the Cases 1, 2 and 3 are reached in 6000, 1400, and 5000 (s), respectively. It is also observed that the time scale of scouring is different between Case 1 (non-equilibrium sediment transport model) and Case 2

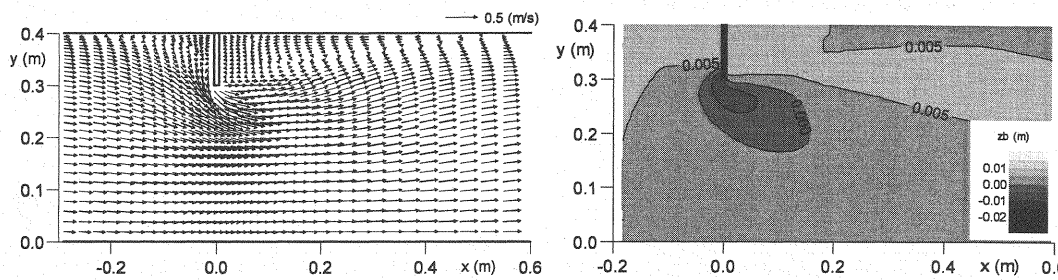

(a) t = 60 (s)

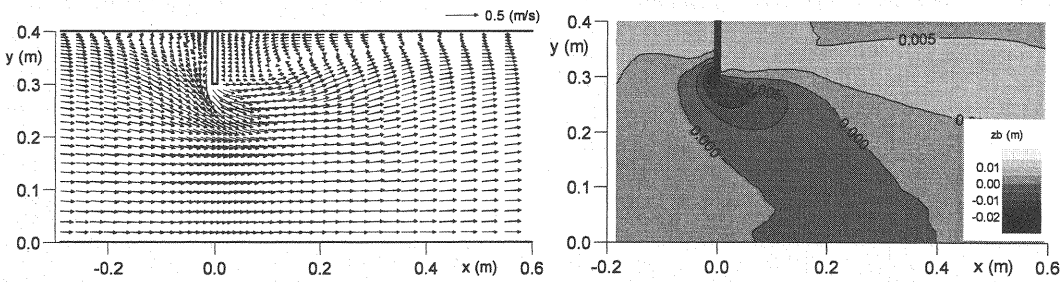

(b) t = 120 (s)

Fig. 8 Temporal variation of flows near bed and bed elevation contours (Case 3)

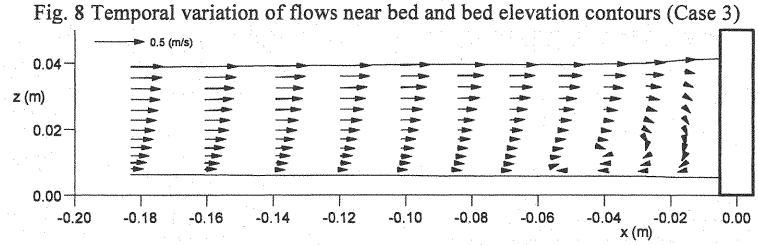

(a) Case 1

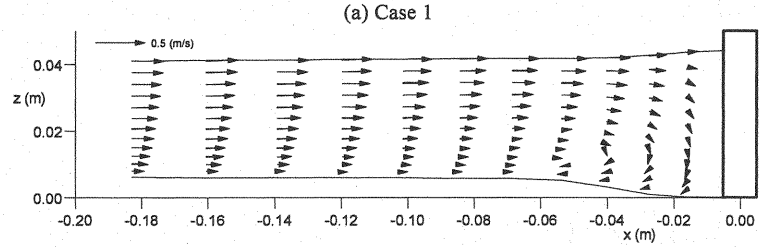

(b) Case 2

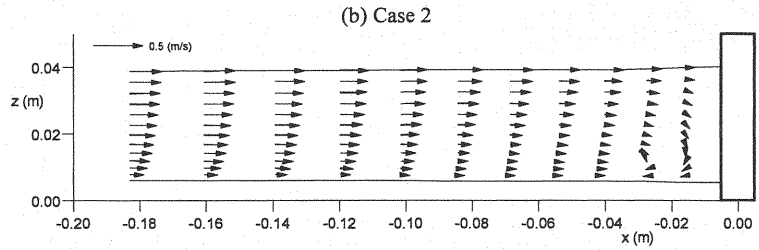

(c) Case 3

Fig. 9 Velocity vectors at section E-E at initial scouring stage (t = 60(s))

(equilibrium sediment transport model); the latter case reached the equilibrium stage faster. To compare the experiments with numerical results on a time scale, a quantitative comparison of a time scale is necessary. The comparison shows that the scour depth for Case 3 is shallowest in all cases. The maximum scour depth in the experiments is reported as 0.09m. The results for the Case 1 and Case 2 are in close agreement with the experimental

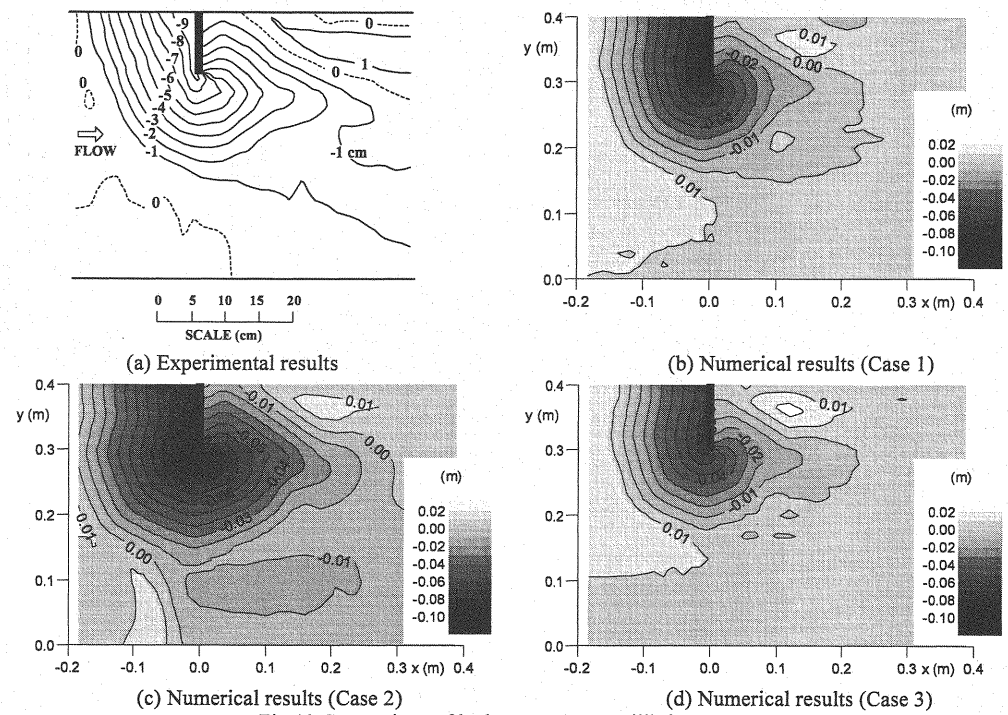

(a) Experimental results

(b) Numerical results (Case 1)

(c) Numerical results (Case 2)

(d) Numerical results (Case 3)

Fig.10 Comparison of bed contours at equilibrium stage

results, while the result for the Case 3 is underestimated.

The flow characteristics and bed level variations in the initial scouring processes are also examined. Figure 3 shows the temporal variation of flow patterns near the bed, as well as bed elevation contours in the initial scouring processes for the Case 1. Scouring starts from the tip of the dike and the sediments along the stream line are picked up due to the flow converging to the tip (Fig. 3(a)). As a result, the sand particles from the tip of the dike to the main stream direction are scoured. While the flow is affected by the bed deformation with the development of scour hole, the water flows along the scour hole, and the flow direction changes only slightly during the initial processes.

Figure 4 and 5 show the velocity vectors of sediment particles at t = 60 (s) and the representative trajectories of sediment movements (pick-up point to the final deposition point) picked up at t = 60(s). Some trajectories are presented in the plots for references. It is observed that the sand particles follow the flow, and some depositions (black) are found behind the dike in the range of x = 0.2 to 0.4 (m).

Figure 6 shows the temporal variations of flow patterns near the bed, as well as the contours of bed elevation for Case 2. The flow structure near the bed for Case 2 at t = 10(s) (Fig.6 (a)) is almost the same as the flow pattern for Case 1 at t = 60 (s). But, as the scour hole develops, the flows as well as considerable amount of sediment depositions are observed behind the dike (Fig.6 (b) t = 60(s)). Moreover, scouring occurs only at the tip of the dike, and the characteristics of bed geometry are found to be different between non-equilibrium (Case1) and equilibrium sediment transport (Case2) models. The temporal changes of bed-load flux vectors are presented in Figure 7. The directions of the bed-load fluxes are changed between t = 10(s) and 60(s) for Case 2, as seen from the results of flow near the bed (Fig. 6).

Figure 8 shows the results of flow patterns near the bed and the contours of the bed elevation for Case 3. Figure 9 illustrates the velocity vectors at the longitudinal E-E sections in all cases, at the initial scouring stage (t = 60(s)). The flow structures in the horizontal plane for the Case 3 (Fig. 8 (a)) are almost the same as in Case 1 and Case 2 (Fig. 3 (a), Fig. 6 (a)), but the flow separation in front of the dike for the Case 3 is weaker (Fig. 8 (b)) than in

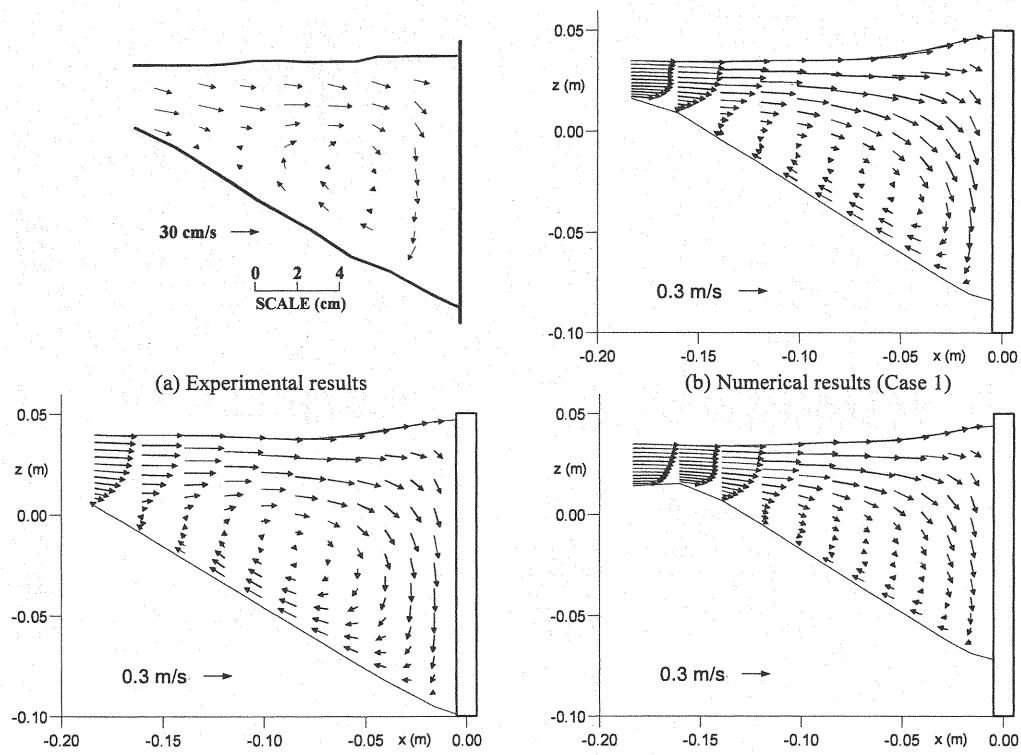

(a) Experimental results

(b) Numerical results (Case 1)

(c) Numerical results (Case 2)

(d) Numerical results (Case 3)

Fig.11 Comparison of velocity vectors at section E-E at equilibrium stage

Case 1 and Case 2. It can be also observed that the scale of the vortex for Case3 (Fig. 9 (c)) is smaller, and the center position of vortex is close to the front of the dike, compared to Case 1 and Case 2 (Fig. 9 (a), (b)).

Figure 10 presents the bed contours in each equilibrium stage. It was found that the maximum scour depth and the deposition region for the Case 1 was slightly smaller than the observations, and the bed contour lines in the numerical simulation were almost parallel to the dike although the experimental result showed inclined lines. However, results show the maximum scour depth in front of dike uniformly, as seen in the experiments. The observed bed topography is also reproduced satisfactorily for the Case 1. The reason for the prediction of inclined bed contour lines may be related to the calculation method of sliding; therefore, further investigation is needed. On the other hand, the result for the Case 2 showed the maximum scour depth only at the tip of the dike, and the deposition and scouring regions were observed near the right bank (x = -0.1 to 0.1 (m)). While the bed elevation around the scour hole in equilibrium stage changed slightly in this case, the shape of scour hole hardly changed. Comparing the bed geometry especially around the dike between the numerical and experimental results, the bed geometry for the Case 2 is not reproduced well. For the Case 3, the maximum scour depth is underestimated. Figure 11 represents a comparison of velocity vectors at section E-E in equilibrium stage. The vortical flows, such as strong downward flow along the front face of spur dike and flow towards the upstream part of scour hole, are pronounced for Case 1 and Case 2. As scour hole develops, the flow near the bed directed upstream affects the pick-up of sediments. However, the vortical flow for the Case 3 (Fig. 11(c)) is weaker compared to Case 1 and Case 2 (Fig. 11 (a), (b)) due to the different turbulence models. Therefore, the volume of sediment pick-up for the Case 3 is less than the Case 1 and 2. This is the reason why the maximum scour depth for Case 3 is underestimated. Considering the results of the shape of scour hole, especially in front of the dike, combination of the non-equilibrium sediment transport model and nonlinear k-ε turbulence model can predict the flow and bed geometry around spur dike

satisfactorily from practical point of view such as computational time. The effects of non-equilibrium and equilibrium conditions of sediments should be examined further by changing the model scale. This will be the subject of future studies. The applicability of LES turbulence model should also be considered as further studies.

CONCLUSIONS

In this study, local scouring around a spur dike was simulated by using different turbulence and bed deformation models. The applicability of models was verified by examining the temporal variation of flow near the bed and variation of bed level. It was found that the time scale of scouring and the bed topography in the initial scouring process, especially near the dike, were different between the non-equilibrium and equilibrium sediment transport model. It can be concluded that the numerical model, combining the non-equilibrium sediment transport model and nonlinear k-ε turbulence model, can predict the flow and bed geometry more accurately. By simulating the flow and local scouring under other hydraulic conditions, the applicability of the model should be further examined, with the inclusion of a suspended load taken into consideration.

REFERENCES

1. Bosch, G. and Rodi, W. : Simulation of vortex shedding past a square cylinder with different turbulence models, *International Journal for Numerical Methods in Fluids*, vol.28, pp.601-616, 1998.
2. Einstein, H.A. : The bed-load function for sediment transportation in open channel flows, *Technical Bulletin*, No.1026, U.S. Dept. of Agriculture, Soil Conservation Service, 1950.
3. Fukuoka, S., Watanabe A. and Nishimura, T. : On the groin arrangement in meandering rivers, *Journal of Hydraulic, Coastal and Environmental Eng.*, No.443/II-18, pp.27-36, 1992 (in Japanese).
4. Fukuoka, S., Nishimura, T., Takahashi, A., Kawaguchi, A. and Okanobu, M. : Design method of submerged groins, *Journal of Hydraulic, Coastal and Environmental Eng.*, No.593/II-43, pp.51-68, 1998 (in Japanese).
5. Fukuoka, S., Watanabe A., Kawaguchi, H. and Yasutake, Y. : A study of permeable groins in series installed in a straight channel, *Annual Journal of Hydraulic Eng.*, vol.44, pp.1047-1052, 2000 (in Japanese).
6. Gatski, T.B. and Speziale, C.G. : On explicit algebraic stress models for complex turbulent flows, *Journal of Fluid Mech.*, vol.254, pp.59-78, 1993.
7. Harlow, F.H. and Welch, J.E. : Numerical calculation of time dependent viscous incompressible flow of fluid with free surface, *Physics Fluids*, vol.8, pp.2182-2189, 1965.
8. Hasegawa, K. : Bank-erosion discharge based on a nonequilibrium theory, *Proc. of JSCE*, No.316, pp.37-50, 1981 (in Japanese).
9. Hirt, C. W. and Cook, J. L. :Calculating three-dimensional flows around structures and over rough terrain, *Journal of Computational Physics*, Vol.10, pp.324-340, 1972.
10. Hosoda, T., Kimura, I. and Onda, S. : Some necessary conditions for a non-linear k-ε model in classified flow Patterns with a singular point, *Proceedings of 2nd International Symposium on Turbulence and Shear Flow Phenomena*, Stockholm, Sweden, vol.3, pp.155-160, 2001.
11. Ikeda, S, Sugimoto T. and Yoshiike T. : Study on the characteristics of flow in channels with impermeable spur dikes, *Journal of Hydraulic, Coastal and Environmental Eng.*, No.656/II-52, pp.145-155, 2000 (in Japanese).
12. Ishigaki, T., Ueno, T., Rahman, M.M. and Khaleduzzaman, A.T.M. : Scouring and flow structure around an attracting groin, *River Flow 2004*, vol.1, pp.521-525, 2004.
13. Iwagaki, Y. : Fundamental study on critical tractive force, (I) Hydrodynamical study on critical tractive force,

Transactions of JSCE, No.41, pp.1-21, 1956 (in Japanese).

14. Iwasa, Y. and Hosoda, T. : Hydraulic analysis of sediment including flows over smooth bed, *Proceedings of International Conference on Physical Modeling of Transport and Dispersion*, IAHR, pp.11B.13-11B.18, 1990.
15. Kimura, I., Hosoda, T. and Onda, S. : Prediction of 3D flow structures around skewed spur dikes by means of a non-linear k-ε model, *River Flow 2002*, vol.1, pp.65-73, 2002.
16. Kimura, I. and Hosoda, T. : A non-linear k-ε model with realizability for prediction of flows around bluff bodies, *International Journal for Numerical Methods in Fluids*, vol.42, pp.813-837, 2003.
17. Kimura, I., Hosoda, T., Onda, S. and Tominaga, A. : Computations of 3D turbulent flow structures around submerged spur dikes under various hydraulic conditions, *River Flow 2004*, vol.1, pp.543-553, 2004.
18. Michiue, M. and Hinokidani, O. : Calculation of 2-dimensional bed evolution around spur-dike, *Annual Journal of Hydraulic Eng.*, vol.36, pp.61-66, 1992 (in Japanese).
19. Muneta, N. and Shimizu, Y. : Numerical analysis model with spur-dike concerning the vertical flow velocity distribution, *Proc. JSCE*, No.497, pp.31-39, 1994 (in Japanese).
20. Nagata, N., Hosoda, T., Nakato, T. and Muramoto, Y. : Three-dimensional numerical model for flow and bed deformation around river hydraulic structures, *Journal of Hydraulic Eng.*, ASCE, vol.131, No.12, pp.1074-1087, 2005.
21. Nakagawa, H., Tsujimoto, T. and Murakami, S. : Non-equilibrium bed load transport along side slope of an alluvial stream. *Proceedings of 3rd International Symposium on River Sedimentation*, Univ. of Mississippi, Miss., pp.885-893, 1986.
22. Olsen N.R.B. and Melaaen, M.C. : Three-dimensional calculation of scour around cylinders, *Journal of Hydraulic Eng.*, vol.123, No.11, pp.962-970, 1993.
23. Olsen, N.R.B. and Kjellesvig, H.M.K. : Three-dimensional numerical flow modeling for estimation of maximum local scour depth, *Journal of Hydraulic Res.*, vol.36, No.4, pp.579-590, 1998.
24. Pope, S.B. : A more general effective viscosity hypothesis, *Journal of Fluid Mech.*, vol.72, pp.331-340, 1975.
25. Sugiyama, H., Akiyama, M. and Matsubara, T. : Numerical simulation of compound open channel flow on turbulence with a Reynolds stress model, *Journal of Hydraulic, Coastal and Environmental Engineering*, No.515/ II-31, pp.55-65, 1995 (in Japanese).
26. Tominaga, A. and Matsumoto, D. : Diverse riverbed figuration by using skew spur-dike groups, *River Flow 2006*, vol.1, pp.683-691, 2006.
27. Yoshizawa, A. : Statistical analysis of the deviation of the Reynolds stress from its eddy viscosity representation, *Physics of Fluids*, vol.27, No.6, pp.1377-1387, 1984.
28. Yossef, M.F.M. and de Vriend, H.J. : Mobile-bed experiments on the exchange of sediment between main channel and groyne fields, *River Flow 2004*, vol.1, pp.127-133, 2004.
29. Yossef, M.F.M. and Rupprecht, R. : Modeling the flow and morphology in groyne fields, *River Flow 2006*, vol.2, pp.1707-1713, 2006.
30. Zhang, H., Nakagawa, H., Muto, Y., Baba, Y. and Ishigaki, T. : Numerical simulation of flow and local scour around hydraulic structures, *River Flow 2006*, vol.2, pp.1683-1693, 2006.

APPENDIX – NOTATION

The following symbols are used in this paper:

A_1, A_2, A_3 = shape coefficients of sand grain for one-, two-, and three-dimensional geometrical properties, respectively;

C_D = drag coefficient;

c_e = coefficient of shielding effect;

C_m = coefficient of added mass;

C_μ, C_1, C_2, C_3, $C_{\varepsilon 1}$, $C_{\varepsilon 2}$ = coefficients for turbulence model;

D = fluid drag force on sediment particle;

D_t = eddy viscosity coefficient;

d = diameter of sediment particle;

F = friction force between sediment particle and bed;

F_0 = constant in pick-up rate formula;

$\mathbf{f}$ = gravitational vector ($\mathbf{f} = (0, 0, -g)$);

f_s = probability density function of step length;

G_* = coefficient of deviation between near-bed velocity vector and sediment movement direction;

g = gravitational acceleration;

g^{ij} = contravariant metric tensor;

J = Jacobian of transformation;

k = kinetic energy of turbulence;

k_p = constant in pick-up rate formula;

k_d = constant;

k_L = ratio of lift force to drag force;

M = turbulence model parameter;

m_p = constant in pick-up rate formula;

n = spatial coordinate perpendicular to s-coordinate;

p = pressure;

p_s = pick-up rate;

$\mathbf{P}_{b1}$, $\mathbf{P}_{b2}$ = unit vectors parallel to local bed surface on (x_1-x_3) and (x_2-x_3) planes, respectively;

$\mathbf{P}_{sed\,(n)}$ = position vector of sediment after n-th step from sediment pick-up;

q_{Bs}, q_{Bn} = bed load transport flux in stream and transversal direction, respectively;

q_B^{ξ}, q_B^{η} = bed load transport flux in generalized curvilinear coordinates;

s = spatial coordinate along the stream line;

S = strain parameter;

S_d, S_p = areas of bed surface mesh projected onto horizontal (x_1-x_2) plane where sediment deposition and pick-up take place, respectively;

$s_{(n)}$ = distance of sediment movement;

t = time;

x_1, x_2, x_3 = Cartesian coordinates (x_3 denotes vertical coordinate);

U^i, U^i_G = contravariant components of fluid and grid velocity, respectively;

$\mathbf{u}$ = fluid velocity vector;

u_* = shear velocity;

u_{bi} = fluid velocity near bed (at the distance of $k_d d$ from bed surface);

u_i, u_{iG} = fluid and grid velocity components in Cartesian coordinates, respectively;

$u_{sed\,i}$, $\mathbf{u}_{sed}$ = velocity in the $\mathbf{p}_{bi}$ direction, and vector of sediment particle movement, respectively;

$-\overline{u_i' u_j'}$ = Reynolds stress tensors;

V_d, V_p = deposition and pick-up volume of sediment, respectively;

W = submerged weight of sediment particle;

z_b = bed elevation;

α = angle between the direction of maximum local bed slope and sediment movement direction;

δ = porosity

ε = ratio of dissipation of turbulent kinetic energy;

Φ = coefficient of side bank slope;

θ_{b1}, θ_{b2} = angles of bed inclination in x_1 and x_2 directions, respectively;

θ_b = local bed slope angle;

$\theta_{b\,\max}$ = critical bed slope angle;

θ_p = angle between $\mathbf{P}_{b1}$ and $\mathbf{P}_{b2}$;

μ_k, μ_s = kinetic and static friction factor, respectively;

λ = average step length;

Λ = averaged step length (=100d);

ν = kinematic viscosity;

ρ, σ = fluid and sediment density, respectively;

σ_k, σ_e = model constants for turbulence model;

τ_{ij} = viscous stress tensors;

τ_*, τ_{*c} = magnitude of dimensionless tractive stress vector and its critical value, respectively;

Ω = rotation parameter;

ξ_1, ξ_2, ξ_3 = generalized curvilinear coordinates; and

Ψ = angle between near-bed velocity vector and sediment movement direction.

(Received Jun 29, 2007 ; revised Sep 28, 2007)